Award Accounts

The Chemical Society of Japan Award for Young Chemists for 2009

Electroactive Nanotubes from π-Conjugated Discotic Molecules

Yohei Yamamoto†

ERATO–SORST Nanospace Project, Japan Science and Technology Agency, 2-3-6 Aomi, Koto-ku, Tokyo 135-0064

Received September 22, 2010; E-mail: yamamoto@ims.tsukuba.ac.jp

Self-assembly of π-conjugated molecules is attractive for construction of well-defined, nanometer-scale electroactive materials. This account describes our developments on self-assembled nanotubes from Gemini-shaped hexa-*peri*-hexabenzocoronenes (HBCs). At first, detailed molecular arrangement in the nanotube is presented, which is perfectly revealed by a synchrotron radiation X-ray diffraction analysis of a macroscopic fiber consisting of highly aligned HBC nanotubes. Next, electroconductive properties of the HBC nanotubes are investigated. By means of direct current and noncontact methods, anisotropic charge-transport properties in the nanotubes are confirmed. The effect of the surface oligoether chains on intertubular conduction is also examined by field-effect transistor measurements. Finally, optoelectronic applications are developed by constructing newly designed nanotubes. These nanotubes possess a coaxial configuration, where an electron-donating graphitic bilayer of π-stacked HBC arrays is laminated by an electron-accepting molecular layer. Due to the molecular-layer donor/acceptor heterojunction, the nanotubes exhibit remarkable photoconduction and photovoltaic outputs. Furthermore, the optoelectronic properties are modulated by changing the density of electron acceptors on the nanotube surfaces by coassembly of multiple components or utilizing photochromism. These results will advance to electronic and optoelectronic applications of supramolecular nanomaterials.

1. Introduction

Control of molecular arrangement is important for enhancing the performance of organic electronics devices. For example, to achieve a high charge carrier mobility in organic field-effect transistors (FETs), π-conjugated molecules should order with preferably large overlap of their π-electronic clouds to form charge-transport pathways between electrodes.[1] Furthermore, for obtaining high photoelectric conversion efficiency in organic thin-film solar cells, nanophase segregation of electron donor (D) and acceptor (A) molecular layers with wide D/A heterointerfaces is thought desirable.[2] Recently, much attention has been focused on programmed self-assembly, where molecules are sequentially assembled via intermolecular interactions.[3] The term *programmed self-assembly* is in turn a control of intermolecular interactions, which lead to a construction of molecular assembly with a desired molecular configuration. If one can tailor π-electronic molecules into discrete, ordered, and nanometer-sized objects, the resultant materials are expected to serve as nanoscale electronic components.[4] In particular, one-dimensional (1D) nano-objects possess a unidirectional charge-transport pathway,[5] thereby serving as an effective charge transporter when properly located on electrodes. To date, many supramolecular 1D nanowires, including fibers, rods, tapes, tubes, and coils, have been reported,[3] yet the electronic and optoelectronic functions of these nanowires have not yet been sufficiently developed.

Among π-conjugated molecules, polycyclic aromatic hydrocarbons (PAHs) are considered to be promising molecular electronics components because of their strong tendency to form 1D columnar structures. Some unidirectionally assembled PAHs have been shown to exhibit anisotropic charge- and energy-transport activities. A representative example of PAHs includes hexa-*peri*-hexabenzocoronene (HBC), which consists of thirteen fused benzene rings and can be regarded as one of the smallest graphene fragments. Pioneering work by Müllen and co-workers on the self-assembly of HBC derivatives has shown that HBCs with symmetrically substituted paraffinic side chains form discotic liquid crystalline materials that display high charge-carrier mobility.[6]

In 2004, our group reported that Gemini-shaped HBC amphiphile **1a** (Figure 1a), bearing two dodecyl chains on one side and two triethylene glycol (TEG) chains on the other, self-assembles to form a nanotubular object.[7] The nanotube is characterized by an aspect ratio greater than 1000 and has a uniform diameter and wall thickness of 20 and 3 nm, respectively (Figures 1b and 1c). Further microscopic and spectroscopic studies revealed that the nanotube consists of helically rolled-up bilayer tapes composed of π-stacked HBC units, where the inner and outer HBC layers are connected by interdigitation of the dodecyl side chains, while the TEG chains are located on both sides of the tubular wall. Systematic studies

† Present address: Institute of Materials Science, Graduate School of Pure and Applied Sciences, University of Tsukuba, 1-1-1 Tennodai, Tsukuba, Ibaraki 305-8573

Published on the web December 25, 2010; doi:10.1246/bcsj.20100272

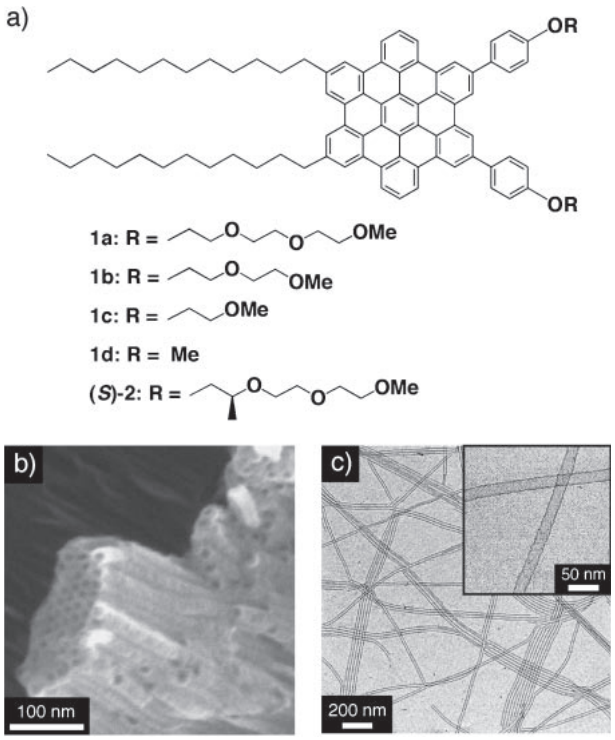

Figure 1. (a) Molecular structures of HBC derivatives **1a**–**1d** and (*S*)-**2**. (b) SEM micrograph of tubularly assembled **1a**. (c) TEM micrograph of tubularly assembled **1a**.

on the self-assembly of Gemini-shaped HBCs showed that analogous HBC derivatives **1b**–**1d** (Figure 1a) with shorter or even no oxyethylene side chains also give nanotubes, revealing that amphiphilicity is not essential for the formation of the nanotubular assembly.[8] These results in turn indicate that the TEG chains may be utilized as a scaffold for anchoring functional groups onto the nanotube surface.[9]

This account begins with our investigation on hierarchical nanotubular structure. The detailed molecular arrangement in the nanotube is revealed by synchrotron radiation X-ray diffraction (XRD) analysis of a fiber sample composed of highly aligned HBC nanotubes. Next, electrical properties of HBC nanotubes are discussed, mainly focusing on the anisotropic intratubular conduction and effect of oligoether chains on the nanotube surface on intertubular conduction. Finally, optoelectronic properties of newly constructed coaxial nanotubes consisting of covalent D–A dyads are presented.

2. Structural Analysis of HBC Nanotubes

X-ray diffraction (XRD) is a powerful method to determine molecular arrangement. Single-crystal XRD analysis is appropriate for the determination of the detailed packing structures of molecules, though it is rather difficult to obtain a single crystal from self-assembled soft nano-objects. However, in the course of study of the self-assembly of HBC derivatives, we happened to notice that nanotubes of **2** (Figure 1a)[10] with one-handed helical chirality can readily be processed into a macroscopic fiber, which is suitable for structural analysis since most of the nanotubes are unidirectionally aligned along the fiber axis.[11]

Thus, a hot 2-methyltetrahydrofuran (MeTHF) solution (50 °C) of (*S*)-**2** (1.5 mg mL^{-1}) was allowed to cool to 25 °C,

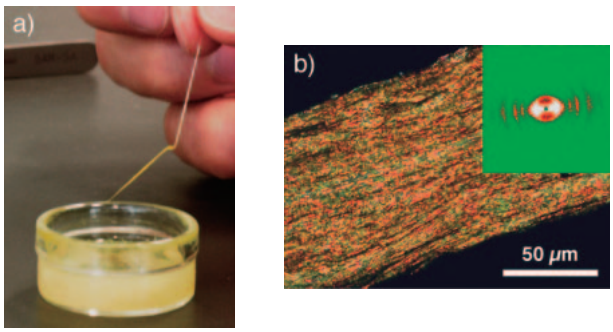

Figure 2. (a) A macroscopic fiber consisting of nanotubes of (*S*)-**2** processed by using a glass hook. (b) POM image of a macroscopic fiber consisting of nanotubes of (*S*)-**2**. Inset shows a 2D SAXD image of the macroscopic fiber located with a vertical direction.

and the resultant suspension was aged for three weeks so that the initially formed nanotubes grew further and were entangled to form large bundles. Then, a glass hook was dipped into this suspension to collect the nanotube bundles and pulled up to stretch the captured aggregate (Figure 2a). This simple *fishing* method allowed processing of several-centimeter-long macroscopic fibers with a diameter of 0.05–0.5 mm. Polarized optical microscopy (POM) of the macroscopic fiber suggested that the majority of the nanotube bundles are oriented unidirectionally along the fiber axis (Figure 2b). The uniaxial orientation of the nanotubes was further confirmed by small-angle X-ray diffraction (SAXD), where several diffraction peaks, assignable to the periodicity of diameter of the nanotube, are observed only for directions perpendicular to the fiber axis (Figure 2b, inset).

Next, wide-angle X-ray diffraction (WAXD) analysis of nanotubes of (*S*)-**2** was conducted using a synchrotron radiation X-ray beam ($\lambda = 1.08$ Å).[8] Figure 3a shows a two-dimensional (2D) WAXD image with a qualified diffraction pattern. At a β-angle (azimuthal angle from the longer-axis direction of the fiber) of 0°, a strong diffraction arc with a *d*-spacing of 0.347 nm was observed (Figure 3b), indicating that the HBC units are π-stacked on top of each other and oriented perpendicular to the longer axis of the macroscopic fiber. Other characteristic diffraction arcs were observed at β-angles of approximately $\pm$45 and $\pm$27°, where the *d*-spacings for the former were $\approx$0.48 and 1.03 nm, while that for the latter was 0.416 nm (Figure 3b). Due to the longitudinal orientation of the nanotubes in the fiber, the diffraction of the fiber allows for elucidating a packing diagram of the assembled HBC molecules. As illustrated in Figure 4, the π-stacked columnar arrays of the HBC molecules are helically stranded, where the central axes of these helical HBC columns are tilted by 45° relative to the longer axis of the tube. The *d*-spacing of 1.03 nm at $\beta = \pm 45°$ corresponds to the intercolumnar distance. In each helical column, the HBC molecules stack with an offset geometry. The *d*-spacings of 0.347 nm at $\beta = 0°$ and $\approx$0.48 nm at $\beta = \pm 45°$ are assigned to the cofacial and center-to-center distances between the π-stacked HBC units. Apparently, the offset helical geometry of the π-stacked HBC units allows the attached phenyl groups to be released from possible steric congestion. In this context, the diffraction peak with a *d*-spacing of 0.416 nm at $\beta = \pm 27°$ is noteworthy. We assume that the phenyl groups may adopt a

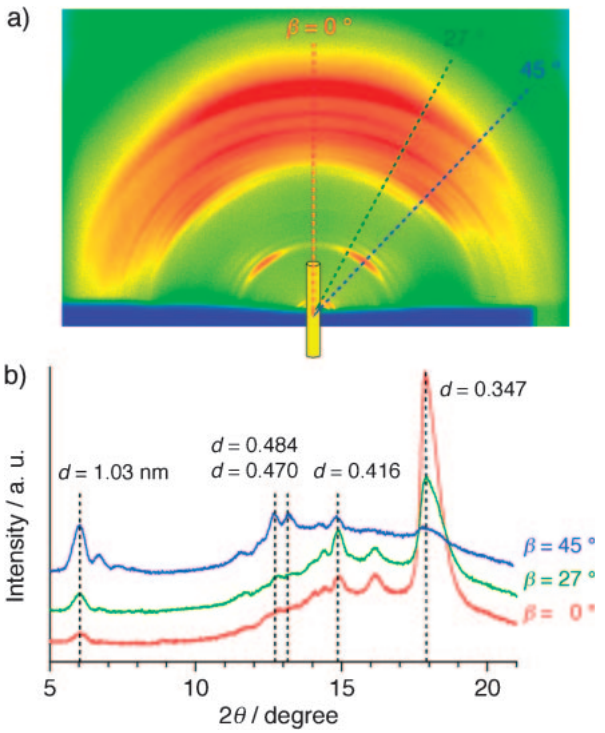

Figure 3. (a) 2D WAXD image of a macroscopic fiber consisting of nanotubes of (*S*)-**2**. (b) X-ray diffraction profiles of the fiber at β-angles of 0 (red), 27 (green), and 45° (blue).

cofacial orientation with a tilting angle of 27° relative to the HBC disk.[12] Thus, the direction of this orientation may determine the handedness of the helical chirality of the nanotube. It is worth noting that powder XRD patterns of HBC nanotubes formed from **1a**–**1d** are roughly identical to that from **2**, indicating that the arrangement of the HBC unit is almost identical for all the nanotubes.

3. Charge-Transport Properties of HBC Nanotubes

3.1 Anisotropic Conduction in the Nanotubes. As revealed by XRD analysis, the wall of the nanotube consists of helical arrays of π-stacked HBC units, which may provide an electrical conduction pathway. Indeed, the nanotube turns electroconductive upon chemical oxidation.[7] Since the nanotubes intrinsically possess 1D structure with a high aspect ratio, we examined anisotropy in the charge carrier transport by making use of the above macroscopic fiber.[11] The nondoped fiber was substantially an insulator, where the resistivities along ($\rho_{//}$) and across ($\rho_{\perp}$) the fiber axis were both greater than 200 MΩ cm. When exposed to iodine vapor, the color of the fiber rapidly turned from yellow to dark brown, and $\rho_{//}$ suddenly dropped and reached after 1 h a constant value of 20 Ω cm. Likewise, $\rho_{\perp}$ decreased upon doping with iodine, however the final value of $\rho_{\perp}$ (280 Ω cm) was more than an order of magnitude larger than $\rho_{//}$ ($\rho_{\perp}/\rho_{//} = 14$). Upon cooling, $\rho_{//}$ and $\rho_{\perp}$ both increased, indicating a semiconducting character of the nanotube (Figure 5a). The difference between $\rho_{//}$ and $\rho_{\perp}$ was larger as the temperature was lower, and a ratio $\rho_{\perp}/\rho_{//}$ of 35 was observed at 55 K. Electron spin resonance (ESR) study of the iodine-doped fiber revealed that

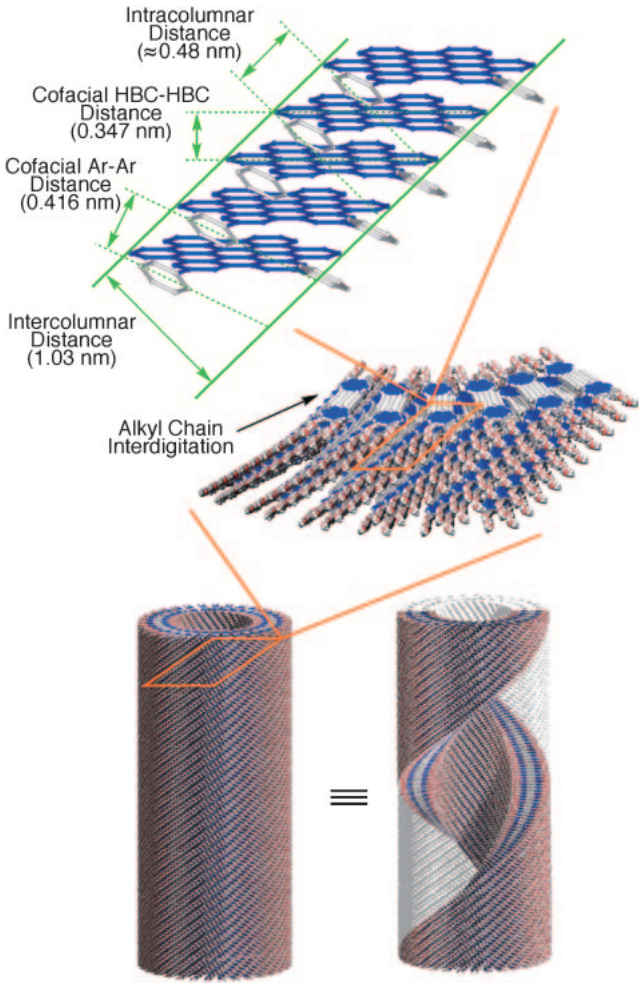

Figure 4. Schematic representations of the hierarchical self-assembled structures of HBC derivative (*S*)-**2**. π-Stacked HBC array (top), bilayer wall (center), and nanotube (bottom).

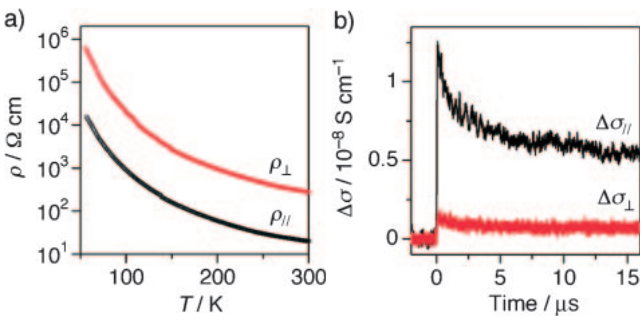

Figure 5. (a) Temperature dependencies of resistivities of an iodine-doped macroscopic fiber consisting of nanotubes of (*S*)-**2** along ($\rho_{//}$, black) and across ($\rho_{\perp}$, red) the fiber axis. (b) Transient conductivities ($\Delta\sigma$) at 298 K of a macroscopic fiber consisting of nanotubes of (*S*)-**2** observed for parallel ($\Delta\sigma_{//}$, black) and perpendicular ($\Delta\sigma_{\perp}$, red) directions to the electric-field vector of the microwave. At time $t = 0$, the fiber was irradiated by a laser pulse ($\lambda = 355$ nm, pulse duration; 5–8 ns) with a photon density of 4.9×10^{15} photons cm^{-2}.

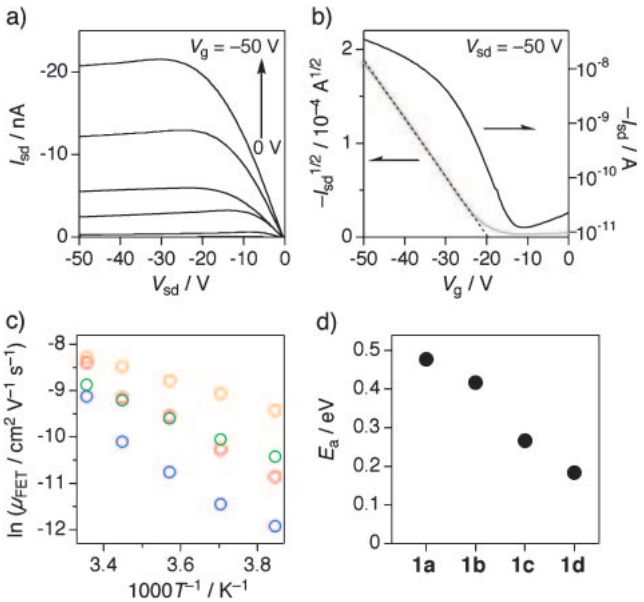

Figure 6. (a) Output and (b) transfer profiles of a thin film of the nanotube of **1a**. (c) Plots of $\ln \mu_{FET}$ versus T^{-1} for thin films of the nanotubes of **1a** (blue), **1b** (red), **1c** (green), and **1d** (orange). (d) Plots of E_a for the nanotubes of **1a**–**1d**.

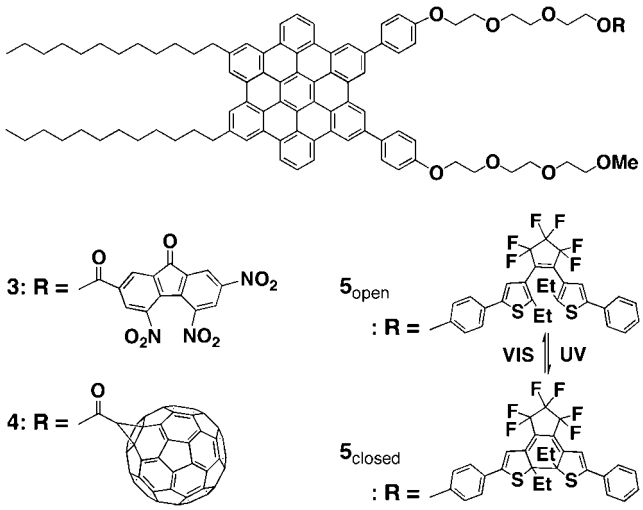

Figure 7. Molecular structures of HBC–TNF **3**, HBC–C_{60} **4**, and HBC–DTE **5**.

g-value and linewidth (ΔH_{pp}) exhibit angular dependencies on the direction of the magnetic field, clearly indicating that the motion of the charge carriers in the nanotubes is anisotropic.[13]

The anisotropic conduction was further confirmed by flash photolysis time-resolved microwave conductivity (FP-TRMC) measurements.[11] FP-TRMC is an electrodeless method for evaluating photocarrier behaviors at a nanometer scale.[14] Figure 5b shows transient conductivities ($\Delta\sigma$) observed for the parallel ($\Delta\sigma_{//}$) and perpendicular ($\Delta\sigma_{\perp}$) directions to the electric field vector of the microwave, where charge carriers are photochemically generated using a third harmonic generation of Nd:YAG laser at 355 nm with an incident photon density of 4.9×10^{15} cm^{-2}. Obviously, $\Delta\sigma_{//}$, observed immediately after the laser flash photolysis, was 9.2 times as large as $\Delta\sigma_{\perp}$. While $\Delta\sigma_{//}$ and $\Delta\sigma_{\perp}$ both increased in proportion to the photon density from 0.5×10^{15} to 4.9×10^{15} cm^{-2}, $\Delta\sigma_{//}$ remained greater than $\Delta\sigma_{\perp}$ ($\Delta\sigma_{//}/\Delta\sigma_{\perp} = 4.9 - 10.6$).

3.2 Effect of Surface Oligoether Chains on Intertubular Conduction. HBC nanotubes turned electroconductive upon chemical oxidation or photoirradiation. In this section, application of the nanotubes to FET devices is presented. Importantly, clear correlation between the length of the oligoether side chains and the field-effect mobilities is observed.[15]

As shown in Figure 6a, a cast film of the nanotubes of **1a** displayed an output profile characteristic of p-type FET, where the source–drain current (I_{sd}) was progressively enhanced as the gate bias voltage (V_g) became increasingly negative. From the transfer profile (Figure 6b), the field-effect mobility (μ_{FET}) and on-to-off current ratio (I_{ON}/I_{OFF}) were determined to be 1.3×10^{-4} cm^2 V^{-1} s^{-1} and 2800, respectively. FET performance of the nanotubes of **1b**–**1d** with different oligoether chain length was further investigated, since the oligoether chains densely cover the nanotube surface, which may suppress intertubular hole hopping. As expected, μ_{FET} improves as the oligoether chains become shorter. For example, at 298 K, the μ_{FET} value observed for nanotubes of **1d** (2.3×10^{-4} cm^2 V^{-1} s^{-1}) was almost twice as large as that observed for the nanotubes of **1a**. This trend was more explicit at a lower temperature such as 260 K, where the μ_{FET} of nanotubes of **1d** (8.1×10^{-5} cm^2 V^{-1} s^{-1}) was even one-order of magnitude greater than that of the nanotubes of **1a** (6.6×10^{-6} cm^2 V^{-1} s^{-1}). As shown in Figure 6d, the activation energy (E_a) for the hole conduction, evaluated from the temperature dependency of μ_{FET} at 298–260 K (Figure 6c), displays a clear correlation to the length of the side chain. For example, E_a of the nanotube of **1d** (0.18 eV) was smaller by a factor of 2.7 than that of the nanotube of **1a** (0.48 eV).

4. Coaxial Nanotubes with Electron Donor/Acceptor Heterojunction

For optoelectronic applications using organic materials, one important issue is how to arrange molecules with a preferable configuration.[2] An ideal configuration for organic photovoltaics (PVs) consists of properly connected hole- and electron-transporting layers (p/n heterojunction) formed from electron-donating (D) and -accepting (A) molecular components, respectively, with neither charge-transfer (CT) complexation nor macroscopic D/A segregation.[2] For the last decade, major progress has been made by the *bulk heterojunction* approach, which integrates, in most cases, electron-accepting molecules such as fullerenes into hole-transporting media composed of π-conjugated polymers.[16] However, despite the practical importance of this approach, the interface for the resulting p- and n-domains is, in principle, hard to tailor at the molecular level.

As a new strategy to solve this essential problem, molecular assembly of covalently or noncovalently connected D–A modules has attracted increasing attention.[17] In this section, our trial to construct a molecular-layer D/A heterojunction is presented using molecularly connected electron donor (HBC) and acceptors such as trinitrofluorenone (TNF),[18,19] C_{60}-fullerene,[20] and dithienylethene (DTE)[21] (Figure 7). Controlled self-assembly of these dyads gives nanotubes with a coaxial

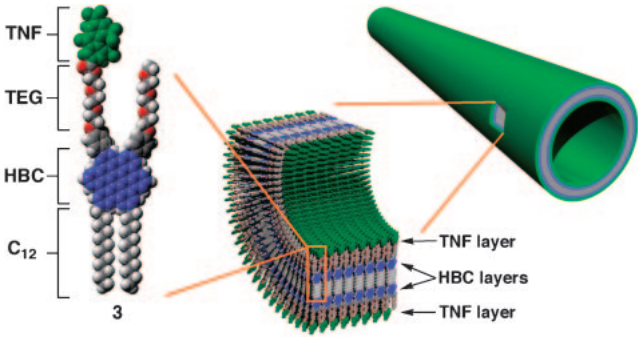

Figure 8. Schematic representations of a self-assembled nanotube of **3** with a coaxial donor–acceptor configuration. A molecular layer of electron-accepting TNF (green) laminates an electron-donating graphitic layer of π-stacked HBC (blue).

configuration, where a molecular layer of electron-accepting TNF, C_{60}, or DTE laminates an electron-donating graphite-like bilayer of π-stacked HBC (Figure 8). This structure creates an extremely wide D/A interface, so that photoirradiation gives rise to an efficient charge separation via photoinduced electron transfer. As a result, these nanotubes exhibit clear photoconduction and photovoltaic outputs.

4.1 Photoconductive Coaxial Nanotubes from HBC–TNF Dyad. TNF is a representative electron-accepting molecule, and has been widely used as a component of photoconductors in xerographic printers. HBC–TNF covalent D–A dyad **3**[18] (Figure 7) was synthesized by oxidative cyclization of TNF-anchored hexaphenylbenzene precursor with $FeCl_3$ in CH_2Cl_2/$MeNO_2$. A tetrahydrofuran (THF) solution of **3** was colored brown, indicating a CT interaction between HBC and TNF in the ground state. Interestingly, depending on the initial concentration of **3**, either nanotubes or microfibers selectively formed. When a THF solution of **3** at a concentration of 0.12 mM was exposed to MeOH vapor at 25 °C, a yellow suspension resulted (Figure 9a, inset). SEM (Figure 9a) and TEM indicated that the yellow-colored substance is composed of nanotubes that have several micrometers long and uniform diameter and wall thickness of 16 and 3 nm, respectively. On the other hand, when the concentration of **3** in THF was 10 times higher (1.2 mM), the diffusion of a MeOH vapor produced a dark-brown precipitate (Figure 9b, inset), which consists only of solid microfibers without hollow space with the diameter ranging from 0.2 to 2 µm (Figure 9b). The concentration-dependent dual-mode self-assembly, thus observed for **3**, most likely originates from a possible competition of the homotropic assembly of the HBC parts with CT complexation (heterotropic assembly) between the HBC and TNF functionalities.

Photoconducting properties of the nanotubes and microfibers of self-assembled HBC–TNF **3** were evaluated by a two-probe method with micrometer-gap electrodes fabricated on a silicon substrate. Current (*I*)–voltage (*V*) profiles of the nanotubes (Figure 9c) showed that the current is remarkably enhanced by a factor of 10^4 upon irradiation. For example, at an applied voltage of +2 V, the photocurrent and dark current of the nanotubes were 4.2 nA and 0.07 pA, respectively. The photocurrent switching was prompt and repeatable by turning on

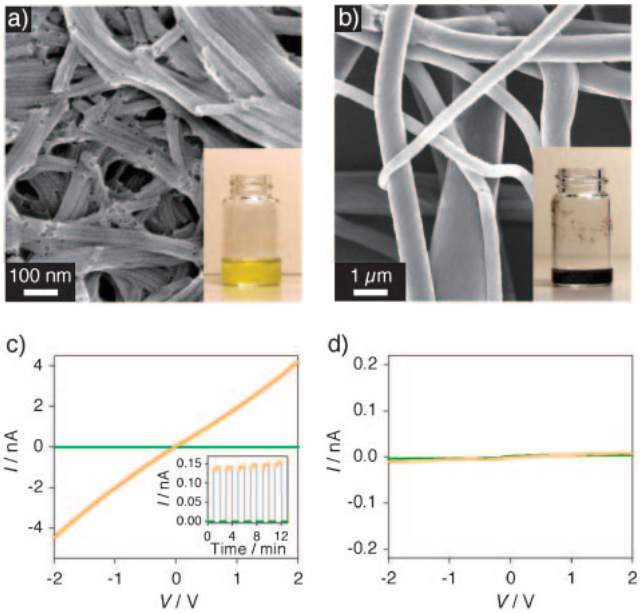

Figure 9. (a) SEM micrograph of an air-dried suspension of the nanotubes of **3**. Inset shows a photograph of a suspension of the nanotubes of **3**. (b) SEM micrograph of an air-dried suspension of the microfibers of **3**. Inset shows a photograph of a suspension of the microfibers of **3**. (c) *I*–*V* profiles at 25 °C of a cast film of the nanotubes of **3** with (orange) and without (green) photoirradiation (λ = 300 to 650 nm). (d) *I*–*V* profiles at 25 °C of a cast film of the microfibers of **3** with (orange) and without (green) photoirradiation (λ = 300–650 nm).

and off the light. In sharp contrast, similar irradiation of the microfibers hardly exhibited photocurrent generation (Figure 9d).

The nanotubes of **3** are characterized by a coaxial configuration, where a molecular layer of electron-accepting TNF laminates an electron-donating graphitic layer of π-stacked HBC (Figure 8). Photoexcitation of the self-assembled HBC should result in the generation of a charge-separated state involving radical cations and anions in the inner and outer layers of the nanotubes, respectively. Such a spatial separation of the charge carriers would prevent their rapid recombination, thereby enabling photoconduction along the nanotubes. In contrast, in the microfiber formed by a CT complexation of the electron-donating and -accepting parts of **3**, recombination of a photogenerated radical ion pair is promoted.

In order to confirm that the current nanotubular structure is indeed optimum for efficient photoconduction, photoconducting properties of the coaxial nanotubes with varying TNF concentration were investigated.[19] Despite the size regimes of the homotropic nanotubes of **3** (16 nm) and **1a** (20 nm) being different from one another, they coassemble uniformly without forming large homotropic domains over a wide range of molar ratio of **3** to **1a**. Interestingly, photoconductivity of the coassembled nanotubes displayed a bell-shaped dependency on the mole fraction of **3** (Figure 10a). The photoconductivity ($\phi\Sigma\mu_{max}$; ϕ and $\Sigma\mu$ are photocarrier generation yield and sum of charge carrier mobility, respectively), evaluated by FP-TRMC measurements, monotonically increases as the mole

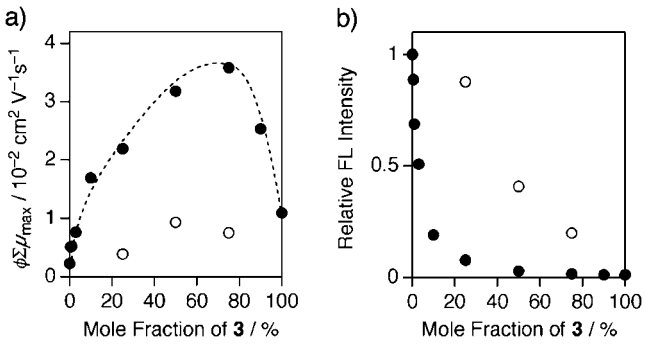

Figure 10. (a) Plots of $\phi\Sigma\mu_{max}$ values for cast films of homotropic and coassembled nanotubes of **1a** and **3** (filled circles) and that of blended nanotubes of **1a** and **3** (open circles) versus mole fractions of **3**. (b) Plot of integral fluorescence intensities for cast films of homotropic and coassembled nanotubes of **1a** and **3** (filled circles) and that of blended nanotubes of **1a** and **3** (open circles) versus mole fractions of **3**.

fraction of **3** increases from 0 to 75% and then decreases progressively. Noteworthy is that only a small amount of **3** (e.g., 10%) gave rise to an even greater $\phi\Sigma\mu_{max}$ value than that of the nanotubes composed of **3** alone. We also found that the fluorescence of **1a** is progressively quenched upon coassembling with **3** (Figure 10b). Hence, the increase in $\phi\Sigma\mu_{max}$ upon increment of the TNF concentration is due to the enhanced HBC-to-TNF electron transfer. On the other hand, the decrease of $\phi\Sigma\mu_{max}$ at the content of **3** from 75 to 100% is possibly because the π-stacked HBC units start to undergo disordering as the bulky TNF densely covers the nanotube surface.

4.2 Photovoltaic Nanotubes from HBC–C_{60} Dyad. In the coaxial nanotubes of HBC–TNF **3**, the TNF layers act as electron-accepting layers, but hardly act as electron transporters. For photovoltaics (PVs), both photogenerated holes and electrons need to be transported. For this purpose, we turned to focus on C_{60}, which is widely used as an electron-transporting component for organic PV devices.[2] HBC–C_{60} covalent D–A dyad **4**[20] (Figures 7 and 8) was synthesized by esterification of the hydroxy group-substituted HBC precursor with metano[60]-fullerene carboxylic acid. Despite the large steric bulk of C_{60}, controlled self-assembly of HBC–C_{60} **4**, by a heat–cool process in toluene (0.2 mM), exclusively gives nanotubes (Figures 11b and 11c). TEM shows that the nanotubes are uniform in diameter and wall thickness (22 and 4.5 nm, respectively; Figure 11d, right). We also tried to coassemble HBC–C_{60} **4** with HBC **1a** (Figures 11a and 11c), in order to know whether heterotropic assembly of **4** and **1a** can take place as in the case of HBC–TNF **3**. SEM and TEM microscopy allowed us to confirm exclusive formation of nanotubes at any molar ratio of **4** to **1a** (Figure 11d). By reference to the homotropic nanotubes of **4** (Figure 11d, right), TEM micrograph of the nanotubes, obtained from a 1:1 mixture of **4** and **1a** (Figure 11d, center), showed that the dark-colored thin region on the nanotube surface, due to the clustering C_{60} pendants, is fragmentary. Therefore, we can conclude that C_{60}-appended **4** is not dispersed uniformly but localized to form domains probably due to an attractive force operative among the C_{60} pendants.

By means of a FET device, we confirmed that the nanotubes of **4** actually behave as both p- and n-type conductors. In the output characteristics (Figures 12a and 12b), the superlinear source–drain current (I_{sd}) was gradually suppressed as the gate bias voltage (V_g) was increased both toward positive and negative. At higher V_g, I_{sd} increased in proportion to an increment of the applied source–drain voltage (V_{sd}) and then leveled off. These behaviors are typical of ambipolar FET.[1b] From the saturated regions in the transfer curves, the electron (μ_e) and hole (μ_h) mobilities of the nanotube of **4** were

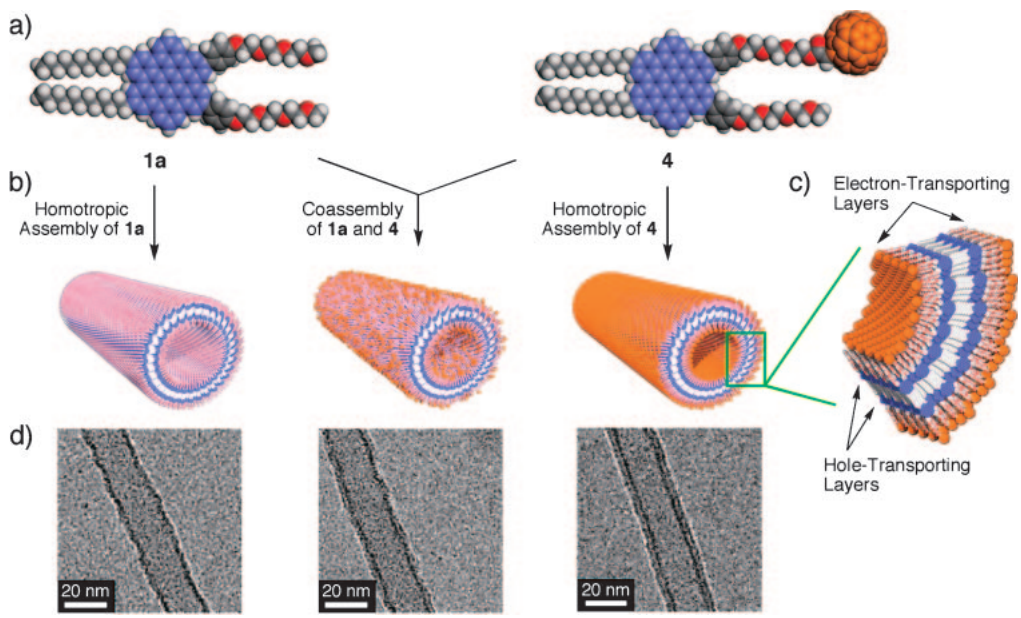

Figure 11. (a) Space-filling models of HBC **1a** and HBC–C_{60} **4**. (b) Schematic representation of the formation of homotropic and coassembled nanotubes of **1a** and **4**. (c) Schematic representation of the wall structure of the nanotubes of **4**. (d) TEM micrographs of air-dried toluene suspensions of the homotropic nanotubes of **1a** (left) and **4** (right), and coassembled nanotubes of **1a** and **4** with a mole fraction of **4** of 50% (center).

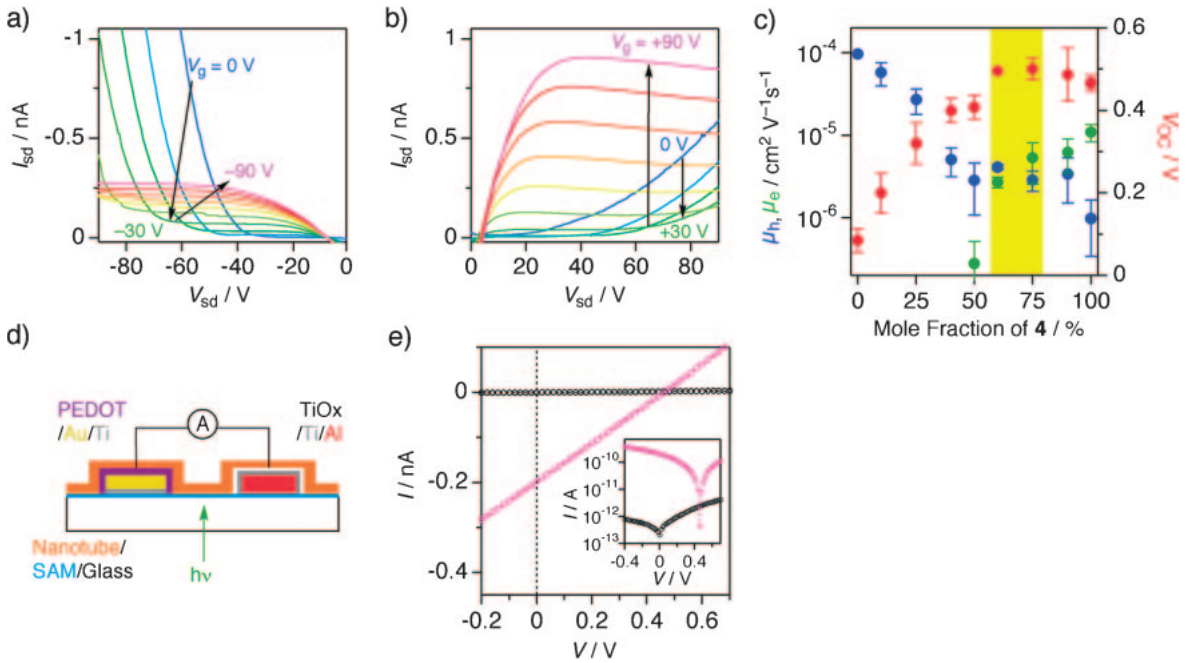

Figure 12. (a, b) Output characteristics of a cast film of the nanotube of **4** for negative (a) and positive (b) gate voltages (V_g). (c) Plots of the electron (μ_e, green) and hole (μ_h, blue) mobilities and open-circuit voltages (V_{OC}, red) versus mole fractions of **4**. (d) Schematic illustration of the device configuration for PV measurements. (e) *I*–*V* and profiles of a cast film of the nanotube of **4** in the dark (black) and upon photoirradiation (pink, $\lambda = 300$–650 nm, 0.39 mW mm^{-2}). Inset shows their semilogarithmic plots.

determined to be 1.1×10^{-5} and 9.7×10^{-7} cm^2 V^{-1} s^{-1}, respectively. A detailed study of the coassembled nanotubes revealed that both μ_e and μ_h are dependent nonlinearly on the nanotube composition (Figure 12c, green and blue, respectively). For example, μ_e decreased gradually as the mole fraction of **4** was decreased from 100 to 60%, and then fell off abruptly thereafter. In particular, no electron mobility was detected when the mole fraction of **4** was lower than 40%, suggesting that the C_{60} cluster on the nanotube surface completely looses an effective continuity for long-range electron transport. On the other hand, as already mentioned, a cast film of the nanotubes of **1a** without C_{60} exhibited only a p-type FET behavior, where μ_h of 1.0×10^{-4} cm^2 V^{-1} s^{-1} is two-orders of magnitude greater than that observed for the homotropic nanotubes of **4**. Nevertheless, only a small increase in the mole fraction of **4** from 0 to 25% resulted in a considerable decrease in μ_h. We believe that the molecular layer of clustering C_{60} prevents hole injection into the graphite-like inner layer from the source electrode. In addition to this, the large steric bulk of C_{60} certainly hampers ideal π-stacking of the HBC units.[19]

Next, we evaluated PV properties of the nanotubes. Since none of the nanotubes upon drop casting could form pinhole-free thin films, necessary for conventional top-contact PV cells, we designed a dedicated device with a side-direction channel (Figure 12d), which may be applicable to 1D nanomaterials. Thus, a toluene suspension of the nanotube of C_{60}-appended **4** was cast onto a fluoroalkyl-coated glass substrate, pre-patterned with PEDOT:PSS/Au/Ti (PEDOT; poly(3,4-ethylenedioxythiophene), PSS; poly(styrenesulfonate)) and TiO_x/Ti/Al electrodes with a 8–15 μm separation. Upon exposure to 300–650 nm light from the backside of the glass substrate, the cast film displayed a photovoltaic response with an open-circuit voltage (V_{OC}) of 0.46 V (Figure 12e). Likewise, PV devices were prepared from the coassembled nanotubes and their performances were investigated. As shown in Figure 12c (red plots), the V_{OC} value increased from 0.09 up to 0.50 V as the mole fraction of **4** was increased from 0 to 75% and then slightly decreased to 0.46 V when the mole fraction of **4** reached 100%. Of particular importance, V_{OC} was maximized at a point where the hole and electron mobilities, as evaluated by FET, were well balanced with one another (mole fraction of **4** = 60–75%; Figure 12c).

4.3 Modulation of Photoconductivity Using Photochromic Function. As shown in the above section, coassembly is effective for controlling the density of the electron-accepting unit at the nanotube surface, which leads to tuning electronic properties of the nanotubes. If the density of the electron acceptors can be controlled by external stimuli, not by coassembly of two components, photoconducting properties may be modulated. Dithienylethene (DTE), a representative photochromic molecule,[22] is attractive for this purpose, because only the closed-form DTE will act as an electron acceptor for HBC.[21]

HBC derivative bearing an open-form DTE pendant ($\mathbf{5}_{open}$, Figure 7) was synthesized by etherification of phenol group-appended DTE with HBC carrying an iodine group at one of the termini of the TEG chains. Controlled self-assembly of $\mathbf{5}_{open}$ into nanotubes took place at 25 °C on standing in $ClCH_2CH_2Cl$ solution (1 mg mL^{-1}, 0.54 mM) for three weeks. The nanotubes in the solid state underwent reversible ring-opening/-closing isomerization at the DTE pendants. Thus, when a $ClCH_2CH_2Cl$ suspension of the nanotubes of $\mathbf{5}_{open}$ was cast onto a quartz plate and air-dried, a yellow-colored thin film was obtained, which displayed absorption bands at 430 and

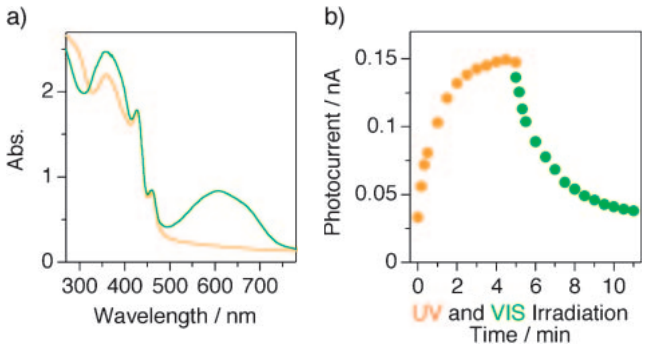

Figure 13. (a) Electronic absorption spectra of a cast film of the nanotubes of $\mathbf{5}_{open}$ before (orange) and after (green) exposure (30 min) to UV light at 310 nm. (b) Change in photocurrent at 25 °C upon excitation at 430–470 nm under an applied voltage of +2 V, where a cast film of the nanotubes of $\mathbf{5}_{open}$ was irradiated with UV light at 310 nm for the initial 5 min (orange) and visible light at 580–650 nm subsequently for the next 6 min (green).

460 nm, characteristic of tubularly assembled HBC units, along with a shoulder band at 310 nm due to the open-form DTE pendants (Figure 13a). Upon exposure to UV light at 310 nm, the film of the nanotubes of $\mathbf{5}_{open}$ changed from yellow to dark green with the appearance of a broad absorption band at 500–750 nm due to the closed form of DTE (Figure 13a). On subsequent irradiation with visible light at 580–650 nm, a spectral profile identical to that observed for the as-cast film of the nanotubes of $\mathbf{5}_{open}$ resulted. It should be noted here that in the forward and backward photoisomerization processes, the positions and intensities of the absorption bands due to the π-stacked HBC units (430 and 460 nm) remained unchanged (Figure 13a), indicating that the columnar HBC arrays in the graphite-like bilayer of the nanotube remain intact during the geometric change of the DTE pendants.

For photoconducting measurements, a cast film of the nanotubes was exposed to visible light at 430–470 nm (light power density, 7.0 mW cm^{-2}) to excite the π-stacked HBC units selectively. The photocurrent, thus observed for the nanotubes of $\mathbf{5}_{closed}$, was 5-fold greater than that of $\mathbf{5}_{open}$. Furthermore, the photocurrent varied with the mole fractions of the open and closed forms of DTE. As is clear from Figure 13b, when the irradiation time for the conversion of $\mathbf{5}_{open}$ into $\mathbf{5}_{closed}$ was longer, the photocurrent gradually became larger and reached a maximum value. On the other hand, when the irradiation wavelength was changed from 310 to 580–650 nm, the photocurrent in turn decreased with time and eventually recovered the initial value. Isomerization of the DTE pendants leads to a change in efficiency of the photoinduced HBC-to-DTE electron transfer, thereby giving rise to an alternation of the photocarrier generation yield. As a consequence, the nanotubes of $\mathbf{5}_{open}$ and $\mathbf{5}_{closed}$ possess different photoconductivities from one another, and furthermore photoisomerization of the DTE pendants allows for modulation of the photoconductivity.

5. Conclusion

Thus far, supramolecular chemistry has mainly focused on how molecules interact with one another in solution and how they assemble into a particular structure. This research pioneers electronic and optoelectronic application of self-assembled nanomaterials by taking full advantage of their characteristics. Significant points in this research include (1) an elaboration of molecular layer donor/acceptor heterojunction into a discrete, nanometer-scale object with a molecular-level precision, (2) optimization of the electronic functions by utilizing a coassembly method, and (3) determination of molecular arrangement in the self-assembled nanotubes. I hope these achievements shed light on new aspects of supramolecular nanomaterials and lead to advancement of supramolecular electronics.

The author sincerely acknowledge Prof. Takuzo Aida (The Univ. of Tokyo) and Dr. Takanori Fukushima (RIKEN) for their comprehensive direction, proper guidance, and enthusiastic discussion of this research. The author thanks members in ERATO and SORST Aida Nanospace Project, especially Dr. Wusong Jin (Donghua Univ., China), Mrs. Atsuko Kosaka (RIKEN), Dr. Guanxin Zhang (Chin. Acad. Sci., China), Dr. Yaning He (Tsinghua Univ., China), and Ms. Yuki Suna (RIKEN) for their never-give-up attitude for the synthesis of the attractive compounds. The author also acknowledges many collaborators inside and outside this project for particular experiments and fruitful discussion.

References

1 a) *Organic Electronics: Materials, Manufacturing and Applications*, ed. by H. Klauk, Wiley-VCH, Weinheim, **2006**. b) J. Zaumseil, H. Sirringhaus, *Chem. Rev.* **2007**, *107*, 1296. c) S. Allard, M. Forster, B. Souharce, H. Thiem, U. Scherf, *Angew. Chem., Int. Ed.* **2008**, *47*, 4070.

2 a) *Organic Photovoltaics: Materials, Device Physics, and Manufacturing Technologies*, ed. by C. Brabec, U. Scherf, V. Dyakonov, Wiley-VCH, Weinheim, **2008**. b) S. Günes, H. Neugebauer, N. S. Sariciftci, *Chem. Rev.* **2007**, *107*, 1324. c) B. C. Thompson, J. M. J. Fréchet, *Angew. Chem., Int. Ed.* **2008**, *47*, 58. d) G. Dennler, M. C. Scharber, C. J. Brabec, *Adv. Mater.* **2009**, *21*, 1323.

3 K. Ariga, J. P. Hill, M. V. Lee, A. Vinu, R. Charvet, S. Acharya, *Sci. Technol. Adv. Mater.* **2008**, *9*, 014109.

4 a) F. J. M. Hoeben, P. Jonkheijm, E. W. Meijer, A. P. H. J. Schenning, *Chem. Rev.* **2005**, *105*, 1491. b) P. Pramod, K. G. Thomas, M. V. George, *Chem. Asian J.* **2009**, *4*, 806.

5 a) A. P. H. J. Schenning, E. W. Meijer, *Chem. Commun.* **2005**, 3245. b) L. Zang, Y. Che, J. S. Moore, *Acc. Chem. Res.* **2008**, *41*, 1596. c) L. C. Palmer, S. I. Stupp, *Acc. Chem. Res.* **2008**, *41*, 1674.

6 a) M. D. Watson, A. Fechtenkötter, K. Müllen, *Chem. Rev.* **2001**, *101*, 1267. b) J. Wu, W. Pisula, K. Müllen, *Chem. Rev.* **2007**, *107*, 718. c) S. Sergeyev, W. Pisula, Y. H. Geerts, *Chem. Soc. Rev.* **2007**, *36*, 1902.

7 J. P. Hill, W. Jin, A. Kosaka, T. Fukushima, H. Ichihara, T. Shimomura, K. Ito, T. Hashizume, N. Ishii, T. Aida, *Science* **2004**, *304*, 1481.

8 W. Jin, Y. Yamamoto, T. Fukushima, N. Ishii, J. Kim, K. Kato, M. Takata, T. Aida, *J. Am. Chem. Soc.* **2008**, *130*, 9434.

9 a) W. Jin, T. Fukushima, A. Kosaka, M. Niki, N. Ishii, T. Aida, *J. Am. Chem. Soc.* **2005**, *127*, 8284. b) J. Motoyanagi, T. Fukushima, A. Kosaka, N. Ishii, T. Aida, *J. Polym. Sci., Part A:*

Polym. Chem. **2006**, *44*, 5120. c) J. Motoyanagi, T. Fukushima, N. Ishii, T. Aida, *J. Am. Chem. Soc.* **2006**, *128*, 4220. d) T. Yamamoto, T. Fukushima, Y. Yamamoto, A. Kosaka, W. Jin, N. Ishii, T. Aida, *J. Am. Chem. Soc.* **2006**, *128*, 14337. e) G. Zhang, W. Jin, T. Fukushima, A. Kosaka, N. Ishii, T. Aida, *J. Am. Chem. Soc.* **2007**, *129*, 719. f) J. L. Mynar, T. Yamamoto, A. Kosaka, T. Fukushima, N. Ishii, T. Aida, *J. Am. Chem. Soc.* **2008**, *130*, 1530. g) T. Yamamoto, T. Fukushima, A. Kosaka, W. Jin, Y. Yamamoto, N. Ishii, T. Aida, *Angew. Chem., Int. Ed.* **2008**, *47*, 1672. h) W. Zhang, W. Jin, T. Fukushima, N. Ishii, T. Aida, *Angew. Chem., Int. Ed.* **2009**, *48*, 4747.

10 W. Jin, T. Fukushima, M. Niki, A. Kosaka, N. Ishii, T. Aida, *Proc. Natl. Acad. Sci. U.S.A.* **2005**, *102*, 10801.

11 Y. Yamamoto, T. Fukushima, W. Jin, A. Kosaka, T. Hara, T. Nakamura, A. Saeki, S. Seki, S. Tagawa, T. Aida, *Adv. Mater.* **2006**, *18*, 1297.

12 W. Pisula, Ž. Tomović, M. D. Watson, K. Müllen, J. Kussmann, C. Ochsenfeld, T. Metzroth, J. Gauss, *J. Phys. Chem. B* **2007**, *111*, 7481.

13 T. Hara, K. Furukawa, T. Nakamura, Y. Yamamoto, A. Kosaka, W. Jin, T. Fukushima, T. Aida, *J. Phys. Soc. Jpn.* **2008**, *77*, 034710.

14 A. Saeki, S. Seki, T. Takenobu, Y. Iwasa, S. Tagawa, *Adv. Mater.* **2008**, *20*, 920.

15 Y. Yamamoto, W. Jin, T. Fukushima, T. Minari, K. Tsukagoshi, A. Saeki, S. Seki, S. Tagawa, T. Aida, *Chem. Lett.* **2009**, *38*, 888.

16 a) J. J. M. Halls, C. A. Walsh, N. C. Greenham, E. A. Marseglia, R. H. Friend, S. C. Moratti, A. B. Holmes, *Nature* **1995**, *376*, 498. b) G. Yu, J. Gao, J. C. Hummelen, F. Wudl, A. J. Heeger, *Science* **1995**, *270*, 1789. c) P. Peumans, S. Uchida, S. R. Forrest, *Nature* **2003**, *425*, 158. d) G. Li, V. Shrotriya, J. Huang, Y. Yao, T. Moriarty, K. Emery, Y. Yang, *Nat. Mater.* **2005**, *4*, 864. e) J. Y. Kim, K. Lee, N. E. Coates, D. Moses, T.-Q. Nguyen, M. Dante, A. J. Heeger, *Science* **2007**, *317*, 222.

17 a) E. Peeters, P. A. van Hal, S. C. J. Meskers, R. A. J. Janssen, E. W. Meijer, *Chem.—Eur. J.* **2002**, *8*, 4470. b) F. Würthner, Z. Chen, F. J. M. Hoeben, P. Osswald, C.-C. You, P. Jonkheijm, J. v. Herrikhuyzen, A. P. H. J. Schenning, P. P. A. M. van der Schoot, E. W. Meijer, E. H. A. Beckers, S. C. J. Meskers, R. A. J. Janssen, *J. Am. Chem. Soc.* **2004**, *126*, 10611. c) W.-S. Li, Y. Yamamoto, T. Fukushima, A. Saeki, S. Seki, S. Tagawa, H. Masunaga, S. Sasaki, M. Takata, T. Aida, *J. Am. Chem. Soc.* **2008**, *130*, 8886. d) A. L. Sisson, N. Sakai, N. Banerji, A. Fürstenberg, E. Vauthey, S. Matile, *Angew. Chem., Int. Ed.* **2008**, *47*, 3727. e) A. Kira, T. Umeyama, Y. Matano, K. Yoshida, S. Isoda, J. K. Park, D. Kim, H. Imahori, *J. Am. Chem. Soc.* **2009**, *131*, 3198.

18 Y. Yamamoto, T. Fukushima, Y. Suna, N. Ishii, A. Saeki, S. Seki, S. Tagawa, M. Taniguchi, T. Kawai, T. Aida, *Science* **2006**, *314*, 1761.

19 Y. Yamamoto, T. Fukushima, A. Saeki, S. Seki, S. Tagawa, N. Ishii, T. Aida, *J. Am. Chem. Soc.* **2007**, *129*, 9276.

20 Y. Yamamoto, G. Zhang, W. Jin, T. Fukushima, N. Ishii, A. Saeki, S. Seki, S. Tagawa, T. Minari, K. Tsukagoshi, T. Aida, *Proc. Natl. Acad. Sci. U.S.A.* **2009**, *106*, 21051.

21 Y. He, Y. Yamamoto, W. Jin, T. Fukushima, S. Saeki, S. Seki, N. Ishii, T. Aida, *Adv. Mater.* **2010**, *22*, 829.

22 a) M. Irie, M. Mohri, *J. Org. Chem.* **1988**, *53*, 803. b) M. Irie, *Chem. Rev.* **2000**, *100*, 1685.

Yohei Yamamoto was born in Fukui, Japan in 1975. He received his B.S. (1998) and M.S. degree (2000) in Inorganic and Physical Chemistry under the direction of Prof. Sumio Kaizaki from Osaka University. He obtained his Ph.D. in Inorganic and Physical Chemistry under the direction of Prof. Tomoji Kawai from Osaka University in 2003. He started his academic carrier as a Japan Society for the Promotion of Science postdoctoral fellow at Osaka University (2003–2004) and The University of Tokyo (2004–2005). In 2005, he joined ERATO "Aida Nanospace" Project, and then moved to ERATO–SORST "Nanospace Project" in 2006. Since 2008, he has been a group leader of the project. His research interests include structure and electronic properties of supramolecular nanomaterials as well as electronic and magnetic properties of inorganic materials. He has received an Award for Encouragement of Research in Polymer Science, The Society of Polymer Science, Japan (2008) and The Chemical Society of Japan Award for Young Chemists (2009).